AD-A163 205 ANALYSIS OF EXPERIMENTAL DATA FOR NEUTRALIZATION OF LOW-ENERGY IONS AT A SURFACE(U) STATE UNIV OF NEW YORK AT BUFFALO DEPT OF CHEMISTRY H LEE ET AL JAN 86 TR-3 1/1

UNCLASSIFIED N00014-86-K-0043 F/G 7/4 NL

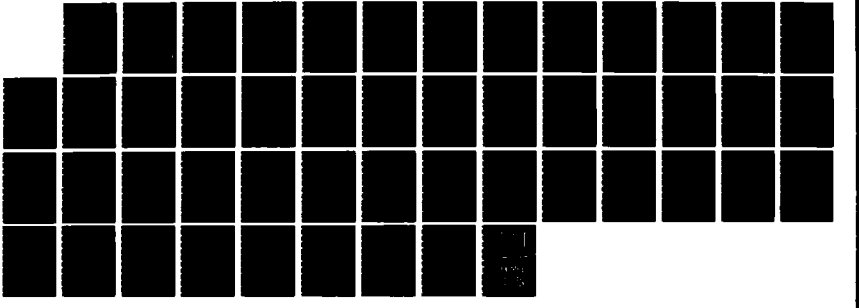

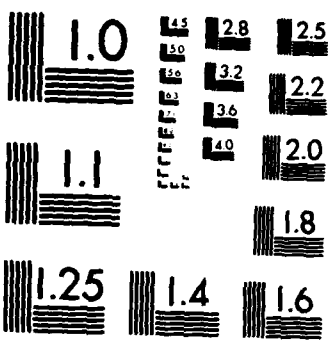

(12)

OFFICE OF NAVAL RESEARCH

Contract N00014-86-K-0043

TECHNICAL REPORT No. 3

Analysis of Experimental Data for Neutralization of Low-Energy Ions at a Surface

by

Hai-Woong Lee and Thomas F. George

Prepared for Publication

in

Surface Science

Departments of Chemistry and Physics
State University of New York at Buffalo
Buffalo, New York 14260

January 1986

6a. NAME OF PERFORMING ORGANIZATION	6b. OFFICE SYMBOL (If applicable)	7a. NAME OF MONITORING ORGANIZATION
Depts. Chemistry & Physics State University of New York		

6c. ADDRESS (City, State and ZIP Code)	7b. ADDRESS (City, State and ZIP Code)
Fronczak Hall, Amherst Campus Buffalo, New York 14260	Chemistry Program 800 N. Quincy Street Arlington, Virginia 22217

8a. NAME OF FUNDING/SPONSORING ORGANIZATION	8b. OFFICE SYMBOL (If applicable)	9. PROCUREMENT INSTRUMENT IDENTIFICATION NUMBER
Office of Naval Research		Contract N00014-86-K-0043

8c. ADDRESS (City, State and ZIP Code)	10. SOURCE OF FUNDING NOS.			
	PROGRAM ELEMENT NO.	PROJECT NO.	TASK NO.	WORK UNIT NO.
Chemistry Program 800 N. Quincy Street Arlington, Virginia 22217				

11. TITLE
Analysis of Experimental Data for Neutralization of Low-Energy Ions at a Surface

12. PERSONAL AUTHOR(S)
Hai-Woong Lee and Thomas F. George

13a. TYPE OF REPORT	13b. TIME COVERED	14. DATE OF REPORT (Yr., Mo., Day)	15. PAGE COUNT
Interim Technical	FROM _____ TO _____	January 1986	

16. SUPPLEMENTARY NOTATION

17. COSATI CODES		
FIELD	GROUP	SUB. GR.

18. SUBJECT TERMS (Continue on reverse if necessary and identify by block number)
ION-SURFACE SCATTERING
LOW ENERGY
NEUTRALIZATION
AUGER/RESONANCE PROCESSES
CHARACTERISTIC VELOCITY
EXPERIMENTAL DATA ANALYSIS

19. ABSTRACT (Continue on reverse if necessary and identify by block number)

When low-energy ions are incident on a solid surface, a large fraction is neutralized via an Auger or resonance process. Some useful information on details of the neutralization process can be obtained by studying the ion fraction of backscattered particles. An accurate evaluation of the charateristic velocity, which determines how fast the ion fraction varies with the incident ion velocity, is expected to be particularly useful. In this paper we give a theoretical analysis of experimental ion yield data that exist in the literature. It is shown that a successful interpretation of the ion yield data can be made by taking into account the variation of the characteristic velocity with respect to the incident ion energy.

SURFACE SCIENCE, in press

ANALYSIS OF EXPERIMENTAL DATA FOR NEUTRALIZATION OF LOW-ENERGY IONS AT A SOLID SURFACE

Hai-Woong Lee
Department of Physics
Oakland University
Rochester, Michigan 48063
U.S.A.

and

Thomas F. George
Departments of Chemistry and Physics
State University of New York at Buffalo
Buffalo, New York 14260
U.S.A.

When low-energy ions are incident on a solid surface, a large fraction is neutralized via an Auger or resonance process. Some useful information on details of the neutralization process can be obtained by studying the ion fraction of backscattered particles. An accurate evaluation of the characteristic velocity, which determines how fast the ion fraction varies with the incident ion velocity, is expected to be particularly useful. In this paper we give a theoretical analysis of experimental ion yield data that exist in the literature. It is shown that a successful interpretation of the ion yield data can be made by taking into account the variation of the characteristic velocity with respect to the incident ion energy.

1. Introduction

Much experimental and theoretical work on neutralization, excitation and deexcitation of ions at a solid surface has been reported in the literature [1-7]. Theoretically, low-energy ($\lesssim$ 5 keV) surface processes have successfully been described by the exponential model of Hagstrum [8-10] in which the rate of surface processes is assumed to decrease exponentially with the ion-surface separation. Experimental electron and photon yield data, in particular, have given strong support to the model. Recently, however, a nonlinear dependence of the logarithm of the ion yield upon the inverse of the initial (or final) ion velocity has been observed by several groups [11-14], in contradiction to the prediction of the model. This is generally believed to be an indication that ions are subject to more than one neutralization mechanism. Theoretical studies in the past have shown that reasonable agreement can still be obtained if one considers, in addition to surface neutralization (Auger or resonance neutralization), neutralization and ionization resulting from atomic collision between the incident ion and a surface atom. Thus, the ion trajectory is conveniently divided into three parts [15-17]: the incoming trajectory, the region of violent atomic collision and the outgoing trajectory. Along the incoming and outgoing trajectories, Auger or resonance neutralization may occur while collisional neutralization and ionization of the atomic type take place in the region of violent collision.

In our earlier work [18] we have introduced a model which presented a different view of the ion-surface interaction. According to the model, the observed nonlinear behavior of the ion yield does not require the introduction of atomic neutralization and ionization. The idea stems from

the observation that the "characteristic velocity" (which determines how fast the scattered ion yield decreases with the ion velocity) is itself a function of the ion energy, resulting in a more complex dependence of the logarithm of the ion yield on the inverse of the ion velocity than a simple linear relationship. Good to excellent agreement has been obtained in the preliminary comparison of our model with experimental ion and photon yield data.

In this paper we further develop the model introduced in ref. 18 so that it can be applied to a wider class of experimental data on nonspecularly as well as specularly reflected particles. We then report the result of an extensive test of our model against experimental ion yield data on various ion-surface combinations. Since for the present work we are interested only in the charge distribution of backscattered particles, there is no need to consider excitation and deexcitation processes which contribute negligibly to the ion yield at low energies of our interest. Our analysis is centered on an accurate determination of the characteristic velocity, necessary for the calculation of the ion yield. It is our hope that the present work gives useful insight into the complex problem of ion-surface interaction at the fundamental level. From the practical viewpoint, the accurate determination of the characteristic velocity should be useful for surface analysis because the characteristic velocity is sensitive to details of the surface such as the molecular composition, electronic state and surface contamination.

In section 2 we give a general description of our model. In particular, we present a detailed analysis of the characteristic velocity for both specularly and nonspecularly reflected particles. Extensive quantitative comparison of the prediction of our model with experimental data

that exist in the literature is presented in section 3. Finally a discussion is given in section 4.

2. Model

A detailed description of our model in terms of rate equations has already been given in ref. 18. Since for the present discussion we are not interested in photon yields or other data related to excitation and deexcitation of ions, surface neutralization (Auger or resonance neutralization) is the only process we need to consider. We also note that atomic neutralization and ionization are not allowed in our model. The rate equation then becomes

$$\frac{dN_1(t)}{dt} = -\Gamma(t)N_1(t), \tag{1}$$

$$\frac{dN_2(t)}{dt} = \Gamma(t)N_1(t), \tag{2}$$

where N_1 is the number of ions, N_2 the number of neutral atoms, and Γ is the neutralization rate assumed to decrease exponentially with respect to the ion-surface separation z,

$$\Gamma(z) = A \exp(-az). \tag{3}$$

Assuming a straight-line, constant-velocity trajectory, i.e., assuming

$$z-z_o = \begin{cases} -v_{i\perp}t\ , & t < 0\ , \\ v_{f\perp}t\ , & t > 0\ , \end{cases} \tag{4}$$

where z_o is the distance of closest approach, and $v_{i\perp}$ and $v_{f\perp}$ are, respectively, the normal components of the initial (v_i) and final (v_f) velocity of the ion, Γ can be expressed in terms of time t as

$$\Gamma(t) = \begin{cases} av_c \exp(av_{i\perp} t) , & t < 0 , \\ av_c \exp(-av_{f\perp} t) , & t > 0 . \end{cases} \tag{5}$$

Here v_c is the characteristic velocity given by

$$v_c = \frac{A}{a} \exp(-az_o) , \tag{6}$$

and, assuming a single binary collision, v_f and v_i are related by

$$v_f = u(\theta) v_i , \tag{7a}$$

where

$$u(\theta) = \frac{1}{1+\frac{m_2}{m_1}} \left[\cos\theta + \left(\sqrt{\frac{m_2}{m_1}^2 - \sin^2\theta} \right) \right] , \tag{7b}$$

θ is the scattering angle, and m_1 and m_2 are the masses of the incident ion and the surface atom, respectively.

We consider the case when the incident particles are singly charged ions, corresponding to the initial condition, $N_1(-\infty) = N$, $N_2(-\infty) = 0$. Eqs. (1) and (2) with this initial condition can immediately be solved to yield

$$N_1(\infty) = N \exp\left[-v_c \left(\frac{1}{v_{i\perp}} + \frac{1}{v_{f\perp}} \right) \right] , \tag{8a}$$

$$N_2(\infty) = N - N \exp\left[-v_c \left(\frac{1}{v_{i\perp}} + \frac{1}{v_{f\perp}} \right) \right] . \tag{8b}$$

The ion fraction f^+ is then given by

$$f^+ \equiv \frac{N_1(\infty)}{N_1(\infty)+N_2(\infty)} = \exp\left[-v_c\left(\frac{1}{v_{i\perp}} + \frac{1}{v_{f\perp}}\right)\right]. \tag{9}$$

In the standard exponential model [8-10], the characteristic velocity v_c is assumed independent of ion energy. Thus, when log f^+ is plotted against $\left(\frac{1}{v_{i\perp}} + \frac{1}{v_{f\perp}}\right)$, one would obtain a straight line and the characteristic velocity could be determined by the slope of the line. We assert, however, that v_c is not independent of energy as can clearly be seen from eq. (6): the characteristic velocity depends on z_o which in turn varies with the ion energy. Hence, according to our model, log f^+ will not vary linearly with $\left(\frac{1}{v_{i\perp}} + \frac{1}{v_{f\perp}}\right)$. An accurate determination of the characteristic velocity v_c and its comparison with experimental data thus provide a severe test of our model. Below we give a detailed analysis of the characteristic velocity and discuss its dependence on the ion velocity and other collision parameters.

Let us first consider specularly reflected particles ($\psi = \theta - \psi$; see fig. 1a). At the distance of closest approach, the total energy available to the ion is approximately $\frac{1}{4} m_1(v_i^2 + v_f^2)$. Assuming that the component of the ion velocity parallel to the surface does not change much during collision, we have

$$\frac{1}{4} m_1(v_i^2 + v_f^2) = \frac{1}{4} m_1(v_i^2 + v_f^2) \cos^2\psi + Be^{-bz_o}. \tag{10}$$

In eq. (10) we have also assumed that the ion-surface interaction at the distance of closest approach is the Born Mayer type. Solving eq. (10) for z_o, we obtain

$$z_o = -\frac{1}{b} \log\left[\frac{m_1(v_i^2+v_f^2) \sin^2\psi}{4B}\right]. \tag{11}$$

Substituting eq. (11) into eq. (6), we obtain the desired expression for v_c for specularly reflected particles:

$$v_c = \frac{A}{a}\left[\frac{m_1(v_i^2+v_f^2)\sin^2\psi}{4B}\right]^{a/b} = \frac{A}{a}\left[\frac{m_1 v_i^2(1+u^2)\sin^2\psi}{4B}\right]^{a/b}. \qquad (12)$$

If we neglect the elastic energy loss of the ion, i.e., if $v_f = v_i$, then eq. (12) reduces to the formula derived in ref. 18. According to eq. (12), the characteristic velocity v_c is an increasing function of the initial (or final) ion velocity at a given angle of incidence ψ, consistent with the observation of Verhey et al [17], Bertrand et al [12] and MacDonald et al [19,20]. Eq. (12) also indicates that the characteristic velocity is an increasing function of the angle of incidence at a given ion energy, consistent with the observation of Bertrand et al [12] and Overbury et al [14].

We now consider nonspecular reflection. The ion which is nonspecularly reflected experiences the repulsive force mainly along the symmetry axis of the trajectory (z′ axis in figs. 1b and 1c). The ion-surface potential in this case is therefore assumed to be given by $V = Be^{-bz'}$ in the neighborhood of the distance of closest approach. For the case $\psi < \theta - \psi$ (fig. 1b), the distance of closest approach is arrived at before the ion reaches the middle point of the trajectory at which most of the elastic energy transfer is assumed to occur. We therefore assume that, at z_o, both the total energy available to the ion and the paralell component of the ion velocity have not changed much from their initial values. Thus, we may write

$$\frac{1}{2} m_1 v_i^2 = \frac{1}{2} m_1 v_i^2 \cos^2\psi + Be^{-bz'_o} . \tag{13}$$

Noting that the z axis and z′ axis make an angle of $\left(\frac{\theta}{2} - \psi\right)$, eq. (13) immediately yields

$$z_o = - \frac{\cos\left(\frac{\theta}{2} - \psi\right)}{b} \log\left(\frac{m_1 v_i^2 \sin^2\psi}{2B}\right), \tag{14}$$

and therefore

$$v_c = \frac{A}{a}\left(\frac{m_1 v_i^2 \sin^2\psi}{2B}\right)^{\frac{a}{b}} \cos\left(\frac{\theta}{2} - \psi\right) \tag{15}$$

The argument goes similarly for the case $\psi > \theta - \psi$ (fig. 1c) except that the ion passes the middle point of the trajectory before it comes closest to the surface, and therefore at z_o the total energy of the ion and the parallel component of the ion velocity are not much different from their final values. We then have

$$\frac{1}{2} m_1 v_f^2 = \frac{1}{2} m_1 v_f^2 \cos^2(\theta - \psi) + Be^{-bz'_o} , \tag{16}$$

$$z_o = - \frac{\cos\left(\psi - \frac{\theta}{2}\right)}{b} \log\left(\frac{m_1 v_f^2 \sin^2(\theta-\psi)}{2B}\right), \tag{17}$$

and

$$v_c = \frac{A}{a}\left(\frac{m_1 v_f^2 \sin^2(\theta-\psi)}{2B}\right)^{\frac{a}{b}} \cos\left(\psi - \frac{\theta}{2}\right) \tag{18}$$

Eqs. (15) and (18) show that, at a given energy and scattering angle, the characteristic velocity v_c decreases as the trajectory moves away from the specular configuration, consistent with the observation of Bertrand et al [12]. One can also observe that, at a given ion energy and incident angle (or exit angle if $\psi < \theta - \psi$), v_c slowly increases as the scattering angle θ is increased. In the next section a detailed quantitative comparison of the analysis given here with experimental data is presented.

3. Comparison with experimental data

3.1. H^+ - C

Hydrogen ions and atoms backscattered from a solid surface generally show a broad energy distribution peaked at a velocity lower than that given by eq. (7a). In such a case our analysis based on the assumption of a single binary collision should apply only to a small fraction of particles that are "kinematically" scattered, i.e., to those that are scattered with velocity given by eq. (7a). Earlier, Overbury et al [14] considered only such particles in their study of H^+-graphite collision. From their experimental ion yield data they calculated the ion fraction of kinematically backscattered particles using scattering cross sections calculated for a screened Coulomb potential. Our analysis therefore can be directly compared with their results.

Our analysis of the 1 keV specular data of Overbury et al was given in ref. 18. With the elastic energy transfer taken into account, we obtained slightly larger values for the parameters $\frac{a}{b}$ and $\frac{A}{a}$ than given in ref. 18: $\frac{a}{b} \cong 0.38$ (compared with 0.37 in ref. 18), $\frac{A}{a} \cong 1.2 \times 10^8$ cm/sec (compared with 1.1×10^8 cm/sec in ref. 18). Here we first show the result of the analysis of the 2 keV specular data of Overbury et al. Shown in table 1 are their calculated values of the ion fraction f^+ and the corresponding values of $v_{f\perp}$, taken from fig. 3 of their paper. Also shown are the values of ψ, $v_{i\perp}$ and v_c that we have calculated. The characteristic velocity v_c was calculated using the relation

$$v_c = \frac{(\log f^+) v_{i\perp} v_{f\perp}}{v_{i\perp} + v_{f\perp}} , \qquad (19)$$

which was obtained by solving eq. (9) for v_c. The characteristic velocity determined this way is the "experimentally determined" v_c because the ion fraction f^+ used in the calculation is taken from experimental data. It can be seen from table 1 that the characteristic velocity v_c is an increasing function of ψ, indicating that the data is at least qualitatively consistent with our model [see eq. (12)]. A stronger support for the model is indicated in fig. 2 where log v_c is plotted against $\log\left(\frac{1+u^2}{2}\sin^2\psi\right)$. According to eq. (12), a linear relationship is expected, which is indeed indicated in the figure. The slope of the line yields the parameter $\frac{a}{b}$, which we estimate to be $\frac{a}{b} \cong 0.38$. We note that the same value of $\frac{a}{b}$ was obtained with the 1 keV specular data, a strong support for the validity of the model. Assuming that the potential energy parameters B and b are given by B = 3 keV and b = 5 Å^{-1} as in our earlier analysis of the 1 keV data, we can now evaluate z_o using eq. (11) and the parameter $\frac{A}{a}$ using the relation $\frac{A}{a} = v_c \exp(az_o)$. The calculated values of z_o and $\frac{A}{a}$ are also shown in table 1. The parameter $\frac{A}{a}$ represents the characteristic velocity at z = 0 and is characteristic of the system being considered. Its values calculated at different ψ should therefore be the same within calculational and experimental uncertainties. We indeed see from table 1 that calculated values of $\frac{A}{a}$ are all fairly close to each other, lending another support to our model. Taking the average we obtain $\frac{A}{a} \cong 1.2 \times 10^8$ cm/sec for the H^+-graphite system. The same value of $\frac{A}{a}$ was obtained with the 1 keV data.

With the parameters $\frac{A}{a} \cong 1.2 \times 10^8$ cm/sec, $\frac{a}{b} \cong 0.38$ and B = 3 keV, we now can calculate the characteristic velocity v_c using eq. (12). The characteristic velocity calculated using eq. (12) represents the value

predicted by our model and thus will be referred to as "theoretically determined" v_c. In table 2 and fig. 3, theoretically determined v_c are shown along with experimentally determined v_c at the incident energies of 1 keV and 2 keV. The agreement between the two sets of values is seen to be very good.

We now look at the nonspecular data of Overbury et al. In table 3 we show values of f^+ and $v_{f\perp}$ as given by Overbury et al along with ψ (or $\theta - \psi$), experimentally determined v_c and theoretically determined v_c that we have calculated for the case E_i (incident ion energy) = 1 keV and $\theta = 90^o$. As before the first set of v_c (experimentally determined v_c) was calculated using eq. (19) with the values of f^+ and $v_{f\perp}$ reported by Overbury et al. The second set of v_c (theoretically determined v_c) was calculated using eq. (15) or eq. (18) with the parameters $\frac{A}{a}$, $\frac{a}{b}$ and B determined above from the analysis of the specular data. The two sets of v_c given in table 3 are shown graphically in fig. 4. Shown also in fig. 4 are experimentally and theoretically determined v_c for the same scattering angle $\theta = 90^o$ but for a different incident energy E_i = 2 keV. For further comparison we show in fig. 5 experimentally and theoretically determined v_c for the case $\theta = 60^o$ and E_i = 1 keV. It is seen that the characteristic velocity determined by our model is generally somewhat lower than the experimentally determined v_c. The general qualitative behavior of the two sets of v_c, however, coincides. For example, both experimentally determined v_c and theoretically determined v_c have a peak at the specular configuration. Considering experimental uncertainties and uncertainties in scattering cross sections and system parameters (especially B = 3 keV and b = 5 Å^{-1}, which are rather arbitrarily chosen), the agreement is good.

3.2. He^+-Cu

The characteristic velocity of the He^+-Cu system has been experimentally investigated by Bertrand et al [12] and Verhey et al [16,17].

The specular data of Bertrand et al [12] shows clearly that v_c is an increasing function of ψ ($= \frac{\theta}{2}$) at a given ion energy. As discussed in the previous section, our model also predicts the increase of v_c with ψ. According to eq. (12), v_c should be proportioned to $\left(\frac{1+u^2}{2} \sin^2\psi\right)^{a/b}$ at a given energy for specular reflection. In table 4 we show experimental values of v_c that we have estimated from the data of Bertrand et al as well as theoretical values calculated using eq. (12). The theoretical values are normalized to the experimental value $v_c \equiv 2.0 \times 10^7$ cm/sec at $E_i = 750$ eV and $\psi = 65^o$ with $\frac{a}{b} = 0.35$, the value which seems to give the best fit to the experimental data. One can observe that a reasonable agreement is achieved between the experimental and theoretical values. The value of $\frac{A}{a}$ can now be estimated by requiring that it yields $v_c \equiv 2.0 \times 10^7$ cm/sec at $E_i = 750$ eV and $\psi = 65^o$. If we take $B = 3$ keV, $b = 5$ Å^{-1} following Hagstrum [8], we obtain $\frac{A}{a} = 3.6 \times 10^7$ cm/sec. If, on the other hand, we choose $B = 1.805$ keV and $b = 3.867$ Å^{-1} according to the table given by Abrahamson [21], we obtain $\frac{A}{a} = 3.0 \times 10^7$ cm/sec.

Bertrand et al have also provided nonspecular data, which indicate that v_c increases as the incidence angle ψ increases from grazing angles toward the specular condition at a given scattering angle θ. This is also consistent with the prediction of our model. Fig. 6 gives the plot of the characteristic velocity v_c calculated using eq. (15) for different values of E_i, ψ and θ. Two different choices of parameters ($\frac{A}{a} = 3.6 \times 10^7$ cm/sec, $B = 3$ keV, $\frac{a}{b} = 0.35$; and $\frac{A}{a} = 3.0 \times 10^7$ cm/sec, $B = 1.805$ keV, $\frac{a}{b} = 0.35$) yielded virtually the same values of v_c, referred to as

theoretically determined v_c in fig. 6. Also shown are experimentally determined v_c which are estimated from the data of Bertrand et al. Unfortunately, only relative magnitudes of v_c can be calculated from their nonspecular data. We therefore have normalized experimentally determined values to $v_c = 1.36 \times 10^7$ cm/sec at $E_i = 750$ eV, $\psi = 28.5^\circ$ and $\theta = 90^\circ$. The agreement between theory and experiment is not very good, especially at $E_i = 1250$ eV. This is mainly due to the fact that the experimental data does not show any visible increase in v_c when the ion energy is increased from 750 eV to 1250 eV, where such behavior is inconsistent not only with our model but also with many other experimental data. We note however that theory and experiment do agree on one major qualitative feature: at given E_i and θ the maximum v_c occurs at the specular configuration. We also note that both theory and experiment agree that, at given E_i and ψ, v_c increases with θ (this, however, is not clearly indicated by the experimentally determined v_c at $E_i = 1250$ eV).

Verhey et al [17] studied the He^+-Cu system and found that v_c is an increasing function of the incident ion energy. However, it is difficult to compare their analysis with ours because they have included collisional neutralization and ionization of the atomic type. We can still obtain theoretical values of v_c and f^+ using eqs. (12) and (9) with the parameters $\frac{A}{a}$, B and $\frac{a}{b}$ for He^+-Cu determined from the data of Bertrand et al. Such a calculation, however, may not be very meaningful because these parameters are expected to vary sensitively with surface contamination. There exists only a remote possibility that surfaces used by two different groups have the same amount of surface contamination.

The same group in another paper [16] has reported the observation made on the He^+-Cu system that, at low incident energy ($E_i = 2$ keV) and

constant θ ($\theta = 30^o$), f^+ is approximately a symmetric function of ψ around the specular configuration $\psi = \frac{1}{2}\theta$. According to our model, a complete symmetry is obtained if $v_f = v_i$, i.e., if $u = 1$. For He^+-Cu, the function u is not much different from 1 ($u \simeq 0.992$) at $\theta = 30^o$, and thus an approximate symmetry is expected, as was observed.

3.3. He^+-Ag, Ne^+-Ag and He^+-Ni

MacDonald et al [19, 20, 22] determined the characteristic velocity for the systems He^+-Ni, He^+-Ag and Ne^+-Ag from the angular distribution of their ion yield measured at constant E_i, θ ($= 90^o$) and ψ, but for different exit trajectories. The exit trajectory was varied by measuring the ion yield in a plane perpendicular to the plane containing the incident beam and surface normal (the incidence plane). The ion fraction measured at an angle ϕ to the incidence plane is given according to eq. (9) by

$$f_\phi^+ = \exp\left[-v_c\left(\frac{1}{v_i \sin\psi} + \frac{1}{v_f \cos\psi \cos\phi}\right)\right]. \qquad (20)$$

If the variation of v_c with ϕ is neglected, we obtain

$$\log \frac{f_\phi^+}{f_{\phi=0^o}^+} = \frac{v_c}{v_f \cos\psi}\left(\frac{1}{\cos\phi} - 1\right). \qquad (21)$$

MacDonald et al obtained a straight line when $\log \frac{f_\phi^+}{f_{\phi=0^o}^+}$ is plotted against $\frac{1}{v_f \cos\psi}\left(\frac{1}{\cos\phi} - 1\right)$, indicating that v_c varies only slightly as a function of ϕ. We therefore neglect the ϕ dependence of v_c in our analysis to follow.

MacDonald and O'Connor [19] obtained the energy dependence of v_c for the systems He^+-Ag and Ne^+-Ag by evaluating the slope of the log $\frac{f^+_\phi}{f^+_{\phi=0^o}}$ vs. $\frac{1}{v_f\cos\psi} \frac{1}{v_f\cos\phi} - 1$ line at different energies. In table 5 we show E_f (scattered ion energy) and v_c taken from the He^+-Ag data of MacDonald and O'Connor along with z_o and $\frac{A}{a}$ calculated as before. Taking the average we obtain $\frac{A}{a} \cong 2.5 \times 10^7$ cm/sec for the He^+-Ag system. Fig. 7 gives the plot of log v_c as a function of log E_f for He^+-Ag and also for Ne^+-Ag. According to eq. (12) one should obtain a linear relationship, which is approximately indicated in the figure. The slope of the line gives $\frac{a}{b}$. From fig. 7 we estimate $\frac{a}{b} = 0.35$ for He^+-Ag and $\frac{a}{b} = 0.44$ for Ne^+-Ag.

3.4. Ne^+-Au

Brongersma et al [15] determined the ion fraction of specularly reflected particles from their experimental data of a 2 keV Ne^+-Au collision. Shown in table 6 are ψ and f^+ taken from their data along with experimentally determined characteristic velocity calculated using eq. (19). We again clearly see that v_c is an increasing function of $\psi = \theta/2$ for specular configurations. In fig. 8 we plot log v_c vs. log $\left(\frac{1+u^2}{2} \sin^2\psi\right)$. The data points fall approximately on a straight line with the slope estimated to be $\frac{a}{b} \cong 0.33$. Thus we see that our model is supported by the experimental data even for the case of heavy-ion incidence. Following Hagstrum [8] we choose B = 36 keV and b = 5 Å^{-1} and calculate z_o using eq. (11) and $\frac{A}{a}$ using the relation $\frac{A}{a} = v_c \exp(az_o)$. The calculated values of z_o and $\frac{A}{a}$ are also shown in table 6. The values of z_o calculated are seen to be significantly larger than the values 0.03 ~ 0.3 Å quoted by Brongersma et al, possibly due to our neglect of multiple scattering which may be significant for the case of Ne^+ incidence. We note, however, that the values of $\frac{A}{a}$ calculated at different ψ remain close from one

another, with the average $\frac{A}{a} \cong 5.85 \times 10^7$ cm/sec. A different choice of parameters, B = 13.625 keV and b = 3.639 Å^{-1}, as suggested by Abrahamson [21], was found to yield similar values of z_o and somewhat lower values of $\frac{A}{a}$ with the average $\frac{A}{a} \cong 4.26 \times 10^7$ cm/sec. The two different sets of the parameters, however, yield virtually the same values of v_c which are shown in fig. 9 along with experimentally determined v_c. The agreement between theory and experiment is surprisingly good, considering that our model based on the assumption of a single binary collision may not accurately describe the Ne^+-Au collision where multiple scattering is probably not negligible.

4. Discussion

The characteristic velocity (more specifically, the characteristic velocity at z = 0) can be a useful parameter for surface analysis because it is sensitive to details of the surface such as the molecular composition and the electronic state. On the other hand, it is its sensitivity to surface contamination [13,23,24] that makes both experimental work and theoretical analysis difficult. For a meaningful determination of the characteristic velocity, the surface under study must be clean, a difficult experimental task. The absolute values of the characteristic velocity determined by our analysis may not represent those characteristic of a clean surface. MacDonald and Martin [22] reported discrepancy in the value of the characteristic velocity for the He^+-Ni system determined by two different methods and ascribed it to the contribution from collisional neutralization and ionization of atomic type. There however seems to exist a possibility that at least a part of the discrepancy arises from different degrees of surface contamination.

The main purpose of the present work is to test the validity of our model introduced in ref. 18 and further developed in section 2 of this paper. It is encouraging that generally good to excellent agreements are obtained between the experimental data and our model, as described in section 3. This indicates that there is much merit in our model according to which surface neutralization is a dominant mechanism that occurs between low-energy ions and a solid surface. Atomic neutralization and ionization and a host of other processes may become important at high energies, but in the low-energy region studied here (a few keV or lower), surface neutralization seems to be the key process that determines the ion fraction of backscattered particles.

Acknowledgements

This research was supported in part by the National Science Foundation under Grant No. CHE-8512406. This research was also supported in part by the Office of Naval Research, the National Science Foundation under Grant No. CHE-8519053 and the Air Force Office of Scientific Research (AFSC), United States Air Force, under Contract F49620-86-C-009. The United States Government is authorized to reproduce and distribute reprints for governmental purposes notwithstanding any copyright notation hereon.

References

[1] Inelastic Ion-Surface Collisions, eds. N.H. Tolk, J.C. Tully, W. Heiland and C.W. White (Academic Press, New York, 1977).

[2] G.M. McCracken, Rep. Prog. Phys. 38 (1975) 241.

[3] E.S. Mashkova and V.A. Molchanov, Rad. Effects 16 (1972) 143.

[4] D.P. Smith, Surface Sci. 25 (1971) 171.

[5] R.J. MacDonald, Advances in Physics 19 (1970) 457.

[6] Physica Scripta T6 (1983), entire issue.

[7] Nucl. Instr. Methods 230 [B2] (1984), entire issue.

[8] H.D. Hagstrum, Phys. Rev. 96 (1954) 336.

[9] H.D. Hagstrum in ref. 1.

[10] A. Cobas and W.E. Lamb, Jr., Phys. Rev. 65 (1944) 327.

[11] E. Taglauer and W. Heiland, Surface Sci. 47 (1975) 234.

[12] P. Bertrand, F. Delannay, C. Bulens and J.-M Streydio, Surface Sci. 68 (1977) 108.

[13] R.S. Bhattacharya, W. Eckstein and H. Verbeek, Surface Sci. 93 (1980) 563.

[14] S.H. Overbury, P.F. Dittner and S. Datz, Nucl. Instr. Methods 170 (1980) 543.

[15] H.H. Brongersma, N. Hazewindus, J.M. van Niewland, A.M.M. Otten and A.J. Smets, J. Vac. Sci. Technol. 13 (1976) 670.

[16] L.K. Verhey, B. Poelsema and A.L. Boers, Rad. Effects 27 (1975) 47.

[17] L.K. Verhey, B. Poelsema and A.L. Boers, Nucl. Instr. Methods 132 (1976) 565.

[18] H.W. Lee and T.F. George, Surface Sci. 159 (1985) 214.

[19] R.J. MacDonald and D.J. O'Connor, Surface Sci. 124 (1983) 423.

[20] R.J. MacDonald, D.J. O'Connor and P. Higginbottom, Nucl. Instr. Methods 230 [B2] (1984) 418.

[21] A.A. Abrahamson, Phys. Rev. 178 (1969) 76.

[22] R.J. MacDonald and P.J. Martin, Surface Sci. 11 (1981) L739.

[23] T.M. Buck, L.C. Feldman and G.H. Wheatley, in Atomic Collisions in Solids, eds. S. Datz et al (Plenum, New York, 1975) Vol. 1, p. 331.

[24] T.M. Buck in ref. 1.

f^+	0.0075	0.0105	0.0115	0.0125	0.017	0.0175	0.018	0.0185	0.024	0.028	0.033	0.034	0.0365	0.0325
$v_{f\perp}(10^7$ cm/sec)	1.05	1.55	2.1	2.5	3.0	3.0	3.0	3.35	3.65	4.3	4.5	4.7	4.7	4.85
ψ(degrees)	9.8	14.7	20.2	24.5	30.3	30.3	30.3	34.6	38.7	48.9	52.6	56.7	56.7	60.3
$v_{i\perp}(10^7$ cm/sec)	1.06	1.57	2.14	2.57	3.12	3.12	3.12	3.52	3.87	4.66	4.91	5.17	5.17	5.38
$v_c(10^7$ cm/sec)	2.58	3.55	4.73	5.55	6.23	6.19	6.14	6.84	7.00	8.00	8.20	8.33	8.15	8.74
z_o(Å)	0.79	0.63	0.51	0.44	0.36	0.36	0.36	0.32	0.28	0.21	0.19	0.17	0.17	0.16
$\frac{A}{a}(10^7$ cm/sec)	11.5	11.8	12.5	12.8	12.4	12.3	12.2	12.5	11.9	11.9	11.8	11.5	11.3	11.8

Table 1. H^+-graphite data for specular conditions at E_i = 2 keV. f^+ and $v_{f\perp}$ values are taken from Overbury et al [14], and ψ, $v_{i\perp}$, v_c, z_o and $\frac{A}{a}$ are calculated as described in this paper.

E_i = 1 keV											
ψ(degrees)	14.7	20.5	25.0	30.7	31.7	35.2	39.1	47.9	53.0	56.0	60.9
$v_c^1(10^7$ cm/sec)	2.67	3.61	4.08	4.99	4.97	5.29	5.45	6.06	6.27	6.38	6.73
$v_c^2(10^7$ cm/sec)	2.78	3.54	4.06	4.67	4.77	5.11	5.45	6.12	6.45	6.62	6.87

E_i = 2 keV														
ψ(degrees)	9.8	14.7	20.2	24.5	30.3	30.3	30.3	34.6	38.7	48.9	52.6	56.7	56.7	60.3
$v_c^1(10^7$ cm/sec)	2.58	3.55	4.73	5.55	6.23	6.19	6.14	6.84	7.00	8.00	8.20	8.33	8.15	8.74
$v_c^2(10^7$ cm/sec)	2.68	3.61	4.56	5.22	6.02	6.02	6.02	6.58	7.05	8.05	8.36	8.67	8.67	8.83

Table 2. Characteristic velocity v_c vs. the incident angle ψ for specular conditions for the H^+-graphite system. v_c^1 and v_c^2 represent experimentally and theoretically determined v_c, respectively.

f^+	0.025	0.0225	0.021	0.0215	0.0215	0.019	0.020	0.0185	0.0175	0.0195	0.018	0.020	0.019	0.0185	0.0195	0.018	0.0195	0.0175	0.016	0.0165	0.0155
$v_{f_\perp}$ (10^7 cm/sec)	3.9	3.8	3.75	3.7	3.5	3.3	3.25	3.2	3.0	2.85	2.85	2.75	2.65	2.4	2.35	2.05	2.05	1.7	1.55	1.4	1.05
ψ(degrees)	14.4	19.3	21.3	23.2	29.6	34.9	36.2	37.4	41.8	45.0	45.0										
$\theta - \psi$ (degrees)										45.0	45.0	43.1	41.2	36.6	35.7	30.6	30.6	25.0	22.6	20.3	15.1
v_c^1(10^7 cm/sec)	3.14	3.98	4.31	4.51	5.13	5.64	5.63	5.80	5.99	5.84	5.96	5.79	5.82	5.69	5.57	5.33	5.22	4.82	4.63	4.28	3.50
v_c^2(10^7 cm/sec)	3.32	3.80	3.98	4.15	4.71	5.15	5.26	5.36	5.72	5.79	5.79	5.46	5.32	4.97	4.90	4.51	4.51	4.06	3.86	3.67	3.21

Table 3. H^+-graphite data for nonspecular conditions at E_i = 1 keV and $\theta = 90^\circ$. f^+ and $v_{f_\perp}$ values are taken from Overbury et al [14]. v_c^1 and v_c^2 represent experimentally and theoretically determined v_c, respectively.

	E_i = 500 eV		E_i = 750 eV		E_i = 1250 eV	
	$\psi = 10^\circ$	$\psi = 65^\circ$	$\psi = 10^\circ$	$\psi = 65^\circ$	$\psi = 10^\circ$	$\psi = 65^\circ$
$v_c^1(10^7$ cm/sec)	0.53	1.7	0.65	2.0	0.99	2.0
$v_c^2(10^7$ cm/sec)	0.56	1.7	0.64	2.0	0.77	2.4

Table 4. Characteristic velocity for specular configurations for the He^+-Cu system. v_c^1 and v_c^2 represent experimentally and theoretically determined v_c, respectively. v_c^2 is normalized to the experimental value of 2×10^7 cm/sec at E_i = 750 eV and $\psi = 65^\circ$.

E_f(eV)	100	200	300	400	400	500	600	600	700	800	900	1000	1000	1100	1200	1300	1400	1400	1500	1600	1700
v_c(10^7 cm/sec)	0.69	0.69	0.88	0.93	1.0	1.18	1.07	1.29	1.15	1.16	1.2	1.2	1.39	1.4	1.45	1.53	1.45	1.55	1.4	1.58	1.56
z_o(Å)	0.81	0.67	0.59	0.53	0.53	0.49	0.45	0.45	0.42	0.40	0.37	0.35	0.35	0.33	0.31	0.30	0.28	0.28	0.27	0.26	0.25
$\frac{A}{a}$(10^7 cm/sec)	2.89	2.26	2.50	2.39	2.57	2.80	2.38	2.87	2.42	2.33	2.31	2.23	2.58	2.52	2.52	2.59	2.39	2.55	2.26	2.49	2.40

Table 5. He^+–Ag data. E_f and v_c values are taken from MacDonald and O'Connor [19], and z_o and $\frac{A}{a}$ are calculated using the method described in this paper.

ψ(degrees)	22.5	30.5	45	53.4	60.5	69.1
f^+	0.009	0.0132	0.025	0.025	0.0266	0.0322
$v_c(10^7$ cm/sec)	1.23	1.48	1.71	1.91	2.01	2.02
z_o(Å)	0.97	0.86	0.74	0.69	0.66	0.64
$\frac{A}{a}(10^7$ cm/sec)	5.93	6.00	5.67	5.88	5.92	5.70

Table 6. Ne^+-Au data for specular conditions at E_i = 2 keV. ψ and f^+ values are taken from Brongersma et al [15], and v_c, z_o and $\frac{A}{a}$ are calculated using the method described in this paper.

Figure Captions

Fig. 1 Specular and nonspecular reflections. ψ and θ are, respectively, the incident angle and scattering angle, the z axis is the surface normal, the z' axis is the axis of symmetry and x denotes the point at which the ion comes closest to the surface.

Fig. 2 $\log v_c$ vs. $\log\left(\frac{1+u^2}{2}\sin^2\psi\right)$ for specular conditions at E_i = 2 keV for the H^+-graphite system.

Fig. 3 Characteristic velocity v_c vs. the incident angle ψ for specular conditions for the H^+-graphite system.

- O experimentally determined v_c at E_i = 1 keV
- X theoretically determined v_c at E_i = 1 keV
- Δ experimentally determined v_c at E_i = 2 keV
- + theoretically determined v_c at E_i = 2 keV

Fig. 4 Characteristic velocity v_c vs. the incident angle ψ for the case $\psi = 90^\circ$ for the H^+-graphite system

- O experimentally determined v_c at E_i = 1 keV
- X theoretically determined v_c at E_i = 1 keV
- Δ experimentally determined v_c at E_i = 2 keV
- + theoretically determined v_c at E_i = 2 keV

Fig. 5 Characteristic velocity v_c vs. the incident angle ψ for the case $\psi = 60^\circ$ for the H^+-graphite system

- O experimentally determined v_c at E_i = 1 keV
- X theoretically determined v_c at E_i = 1 keV

Fig. 6 Characteristic velocity v_c for the He^+-Cu system

○ experimentally determined v_c

× theoretically determined v_c

Fig. 7 log v_c vs. log E_f for He^+-Ag and Ne^+-Ag. v_c and E_f values are taken from the data of MacDonald and O'Connor [19].

Fig. 8 log v_c vs. log $\left(\frac{1+u^2}{2} \sin^2\psi\right)$ for specular conditions at E_i = 2 keV for the Ne^+-Au system.

Fig. 9 Characteristic velocity v_c vs. the incident angle ψ for specular conditions for the Ne^+-Au system.

○ experimentally determined v_c at E_i = 2 keV

× theoretically determined v_c at E_i = 2 keV

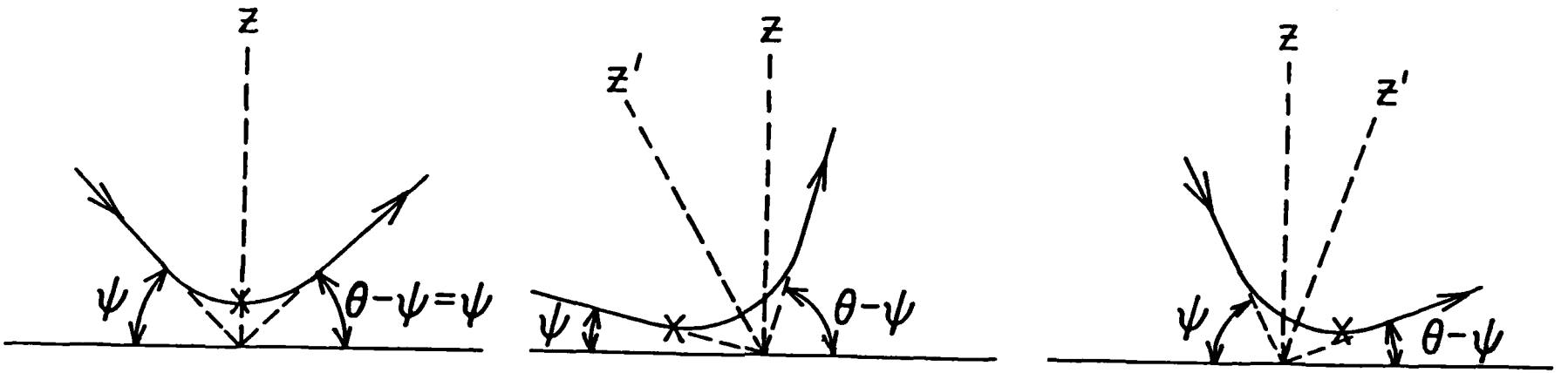
z
ψ
θ-ψ=ψ
z'
z
ψ
θ-ψ
z
z'
ψ
θ-ψ

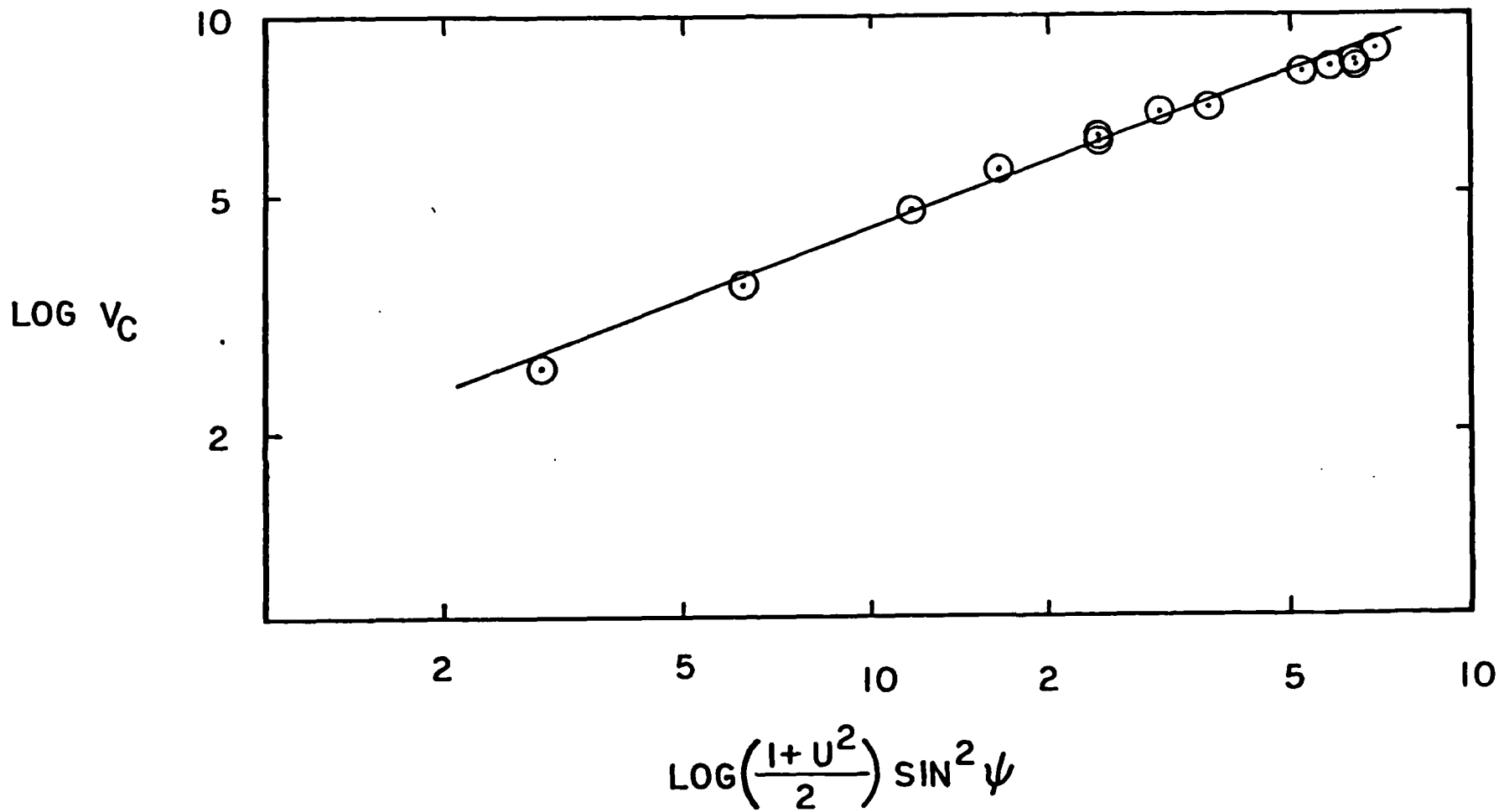
10
5
2
LOG V_C
2
5
10
2
5
10
$\text{LOG}\left(\frac{1+U^2}{2}\right)\text{SIN}^2\psi$

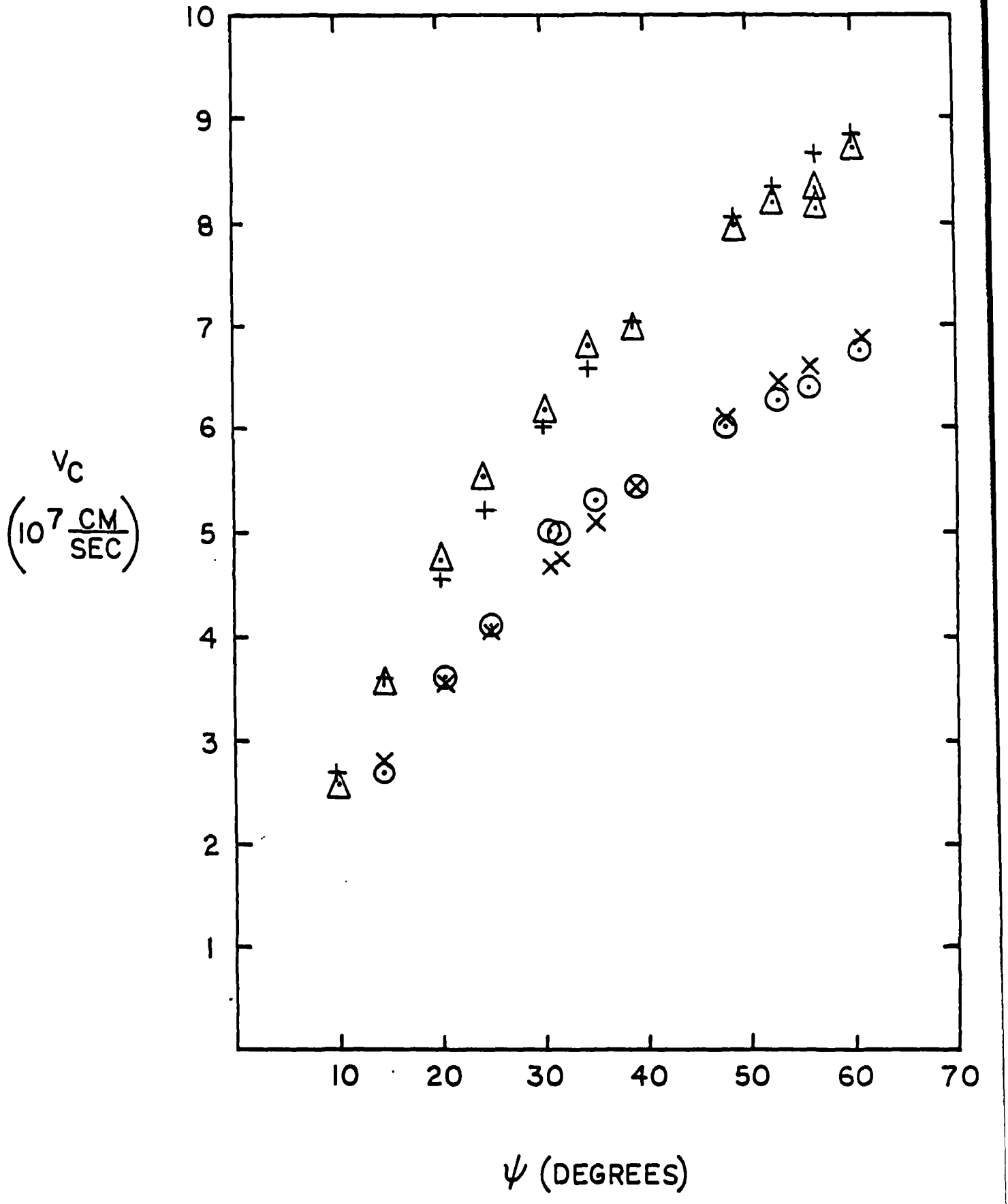
10
9
8
7
6
5
4
3
2
1
10
20
30
40
50
60
70
V_C
$\left(10^7 \frac{CM}{SEC}\right)$
ψ (DEGREES)

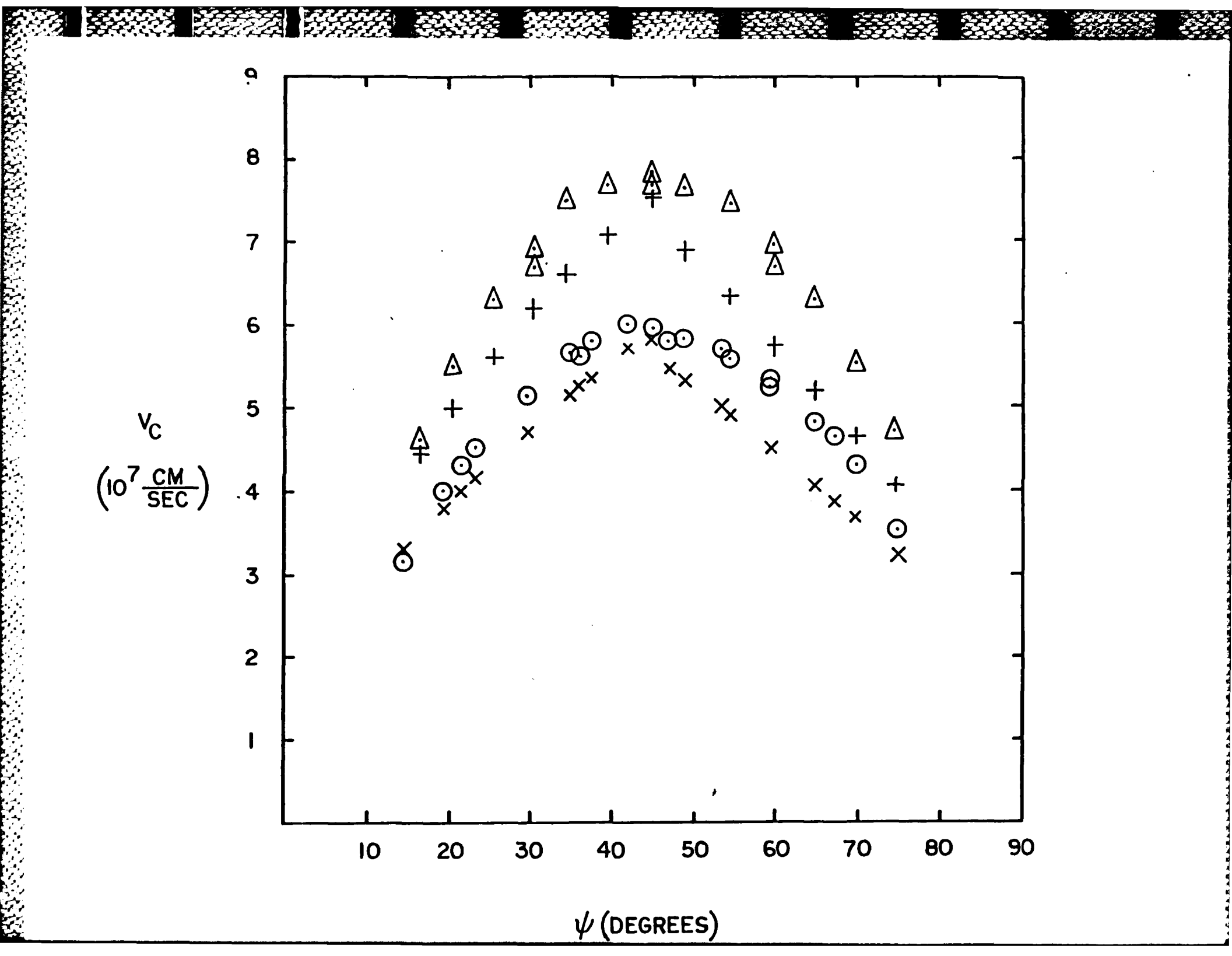
9
8
7
6
5
4
3
2
1
V_C
$(10^7 \frac{CM}{SEC})$
10
20
30
40
50
60
70
80
90
ψ (DEGREES)

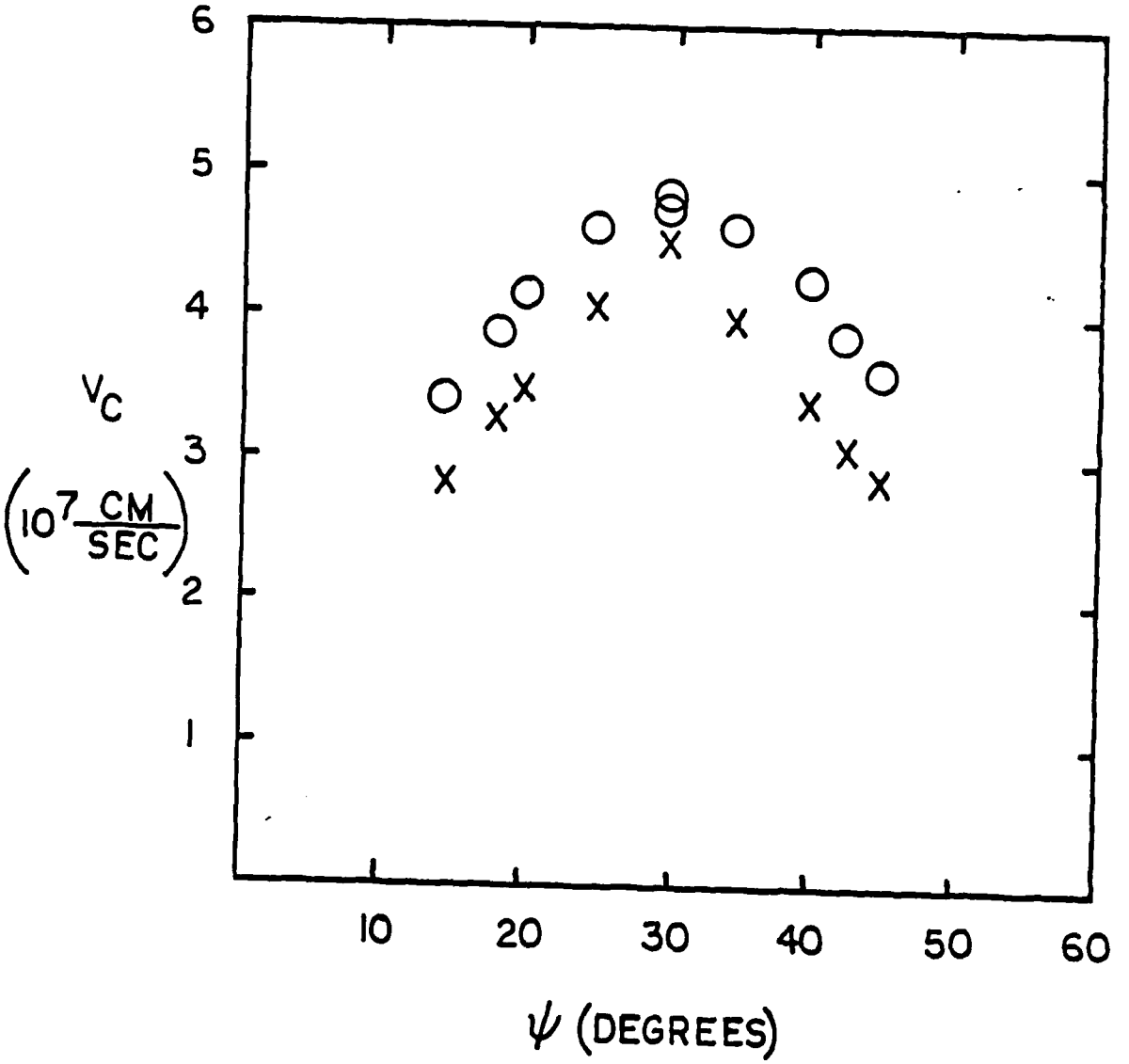
6
5
4
3
2
1
V_C
$\left(10^7 \frac{CM}{SEC}\right)$
10
20
30
40
50
60
ψ (DEGREES)

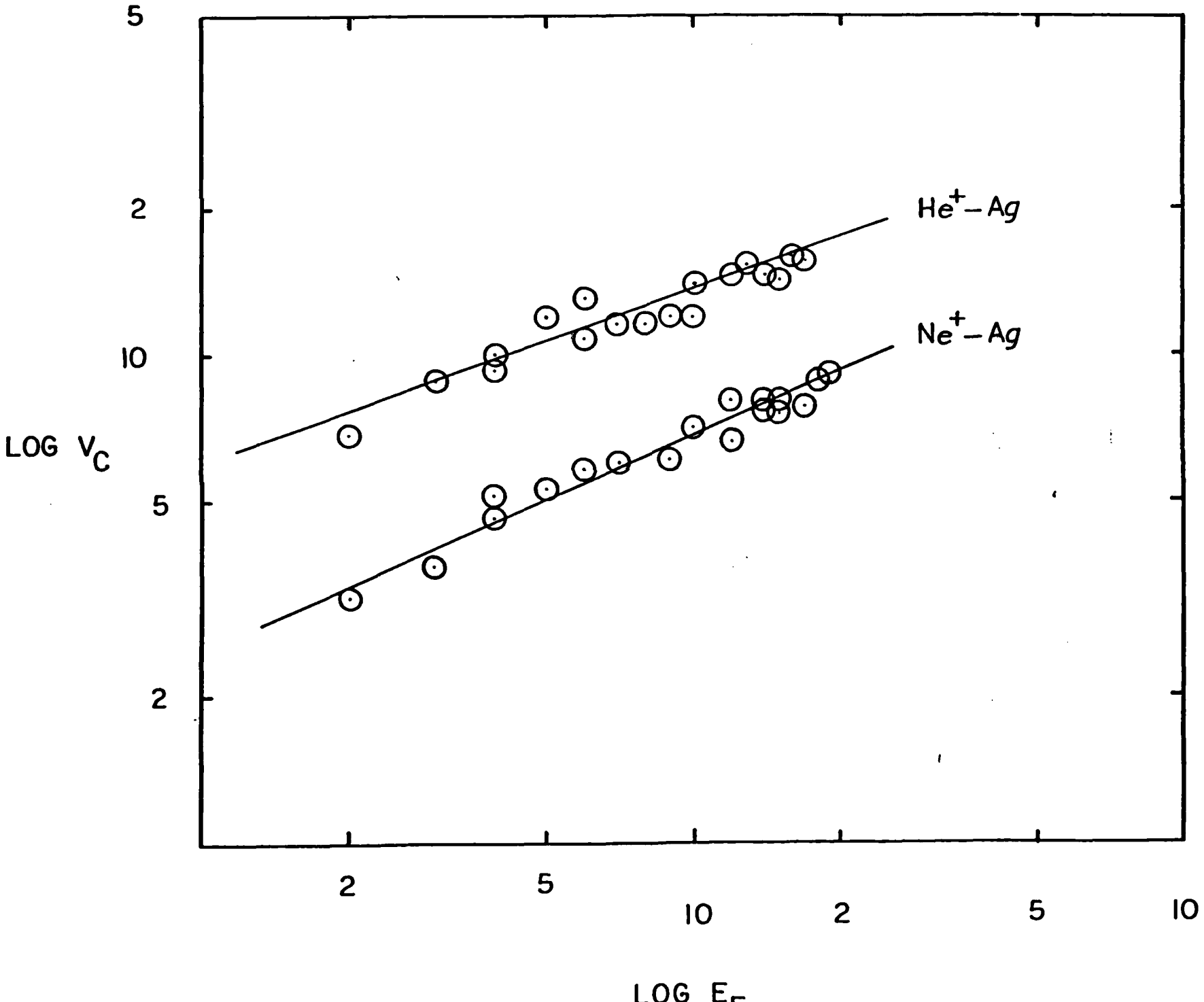
5
2
10
5
2
LOG V_C
$He^+ - Ag$
$Ne^+ - Ag$
2
5
10
2
5
10
LOG E_F

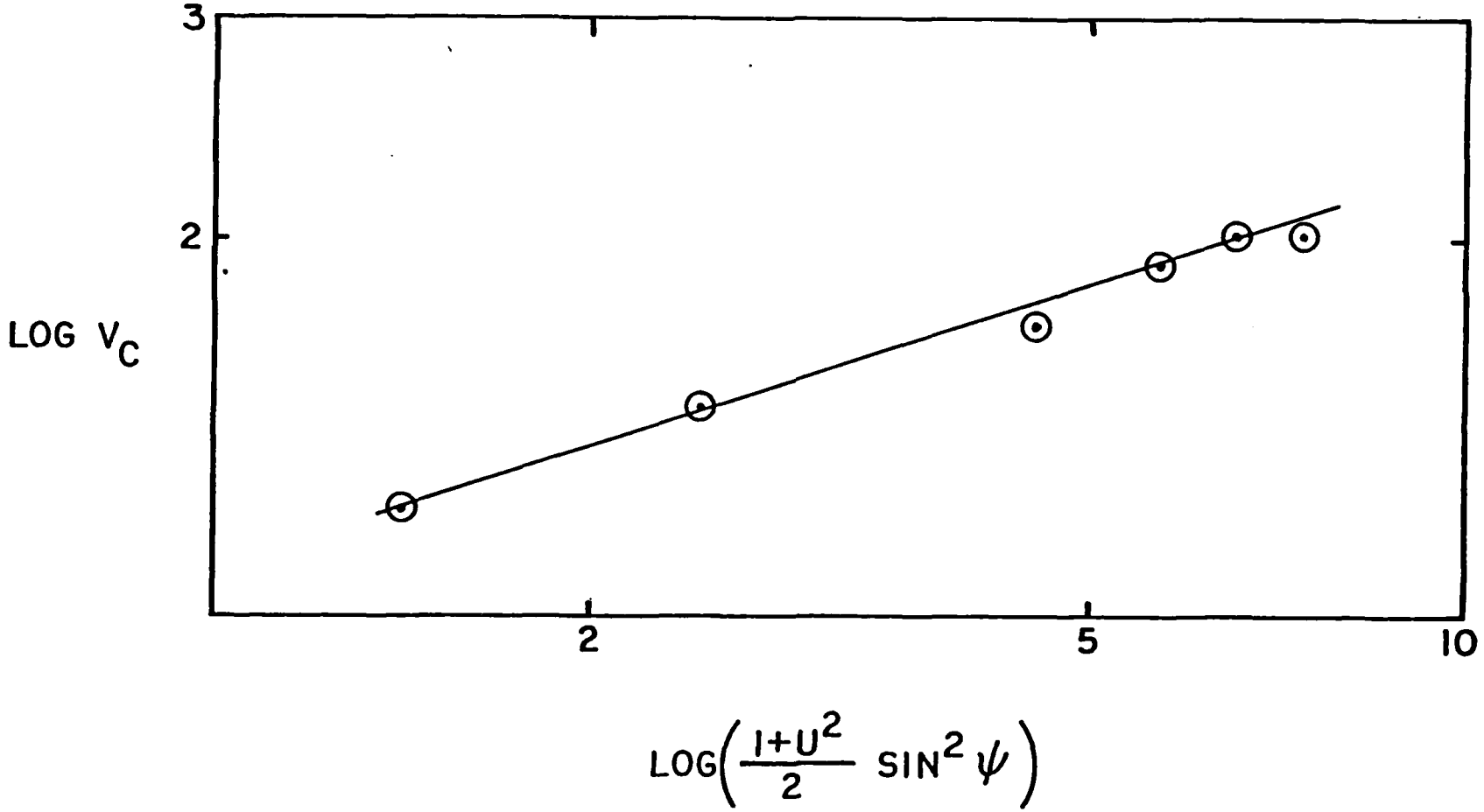
3
2
LOG V_C
2
5
10
$\text{LOG}\left(\frac{1+U^2}{2}\ \text{SIN}^2\psi\right)$

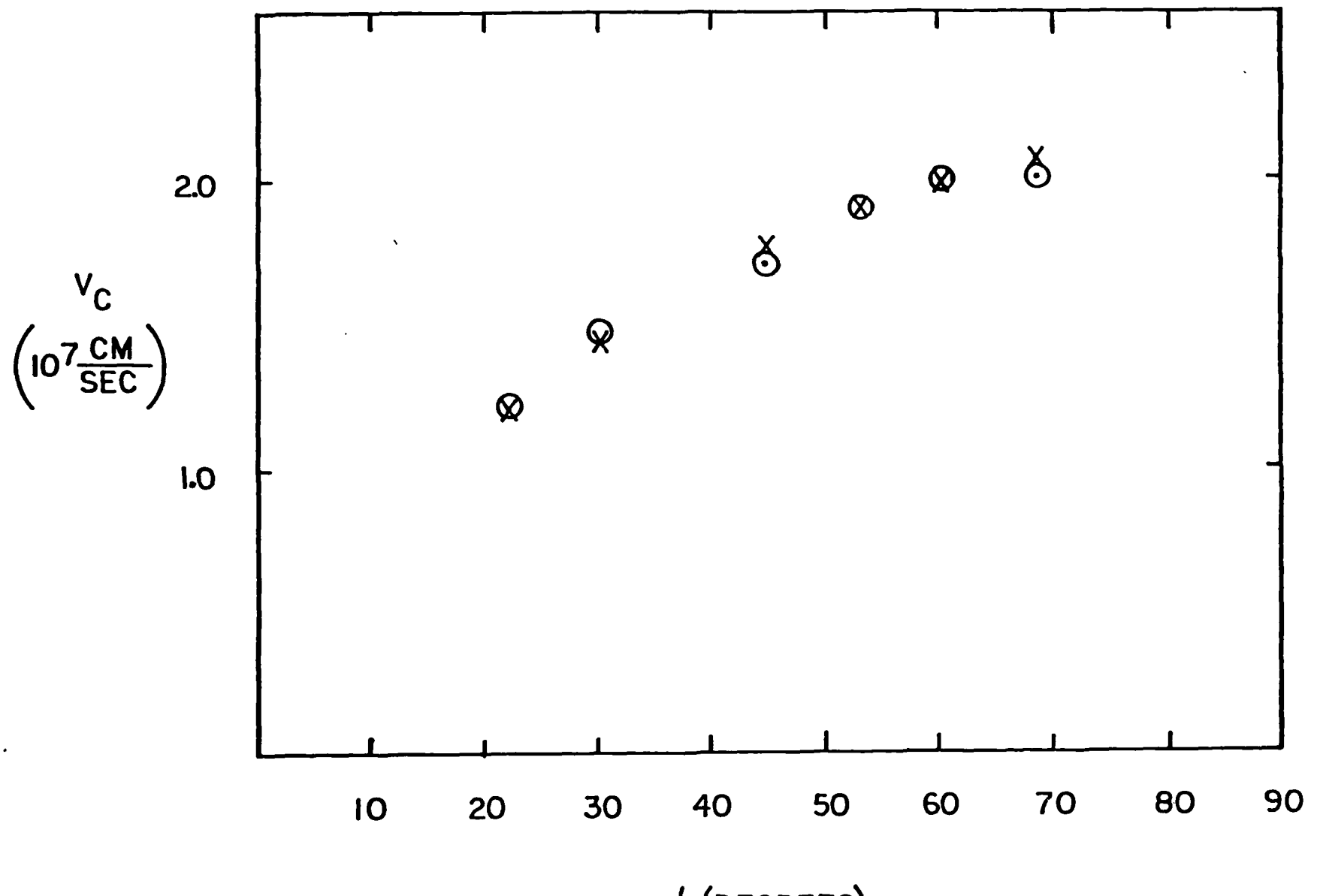
2.0
1.0
V_C
$\left(10^7 \frac{CM}{SEC}\right)$
10
20
30
40
50
60
70
80
90
ψ (DEGREES)

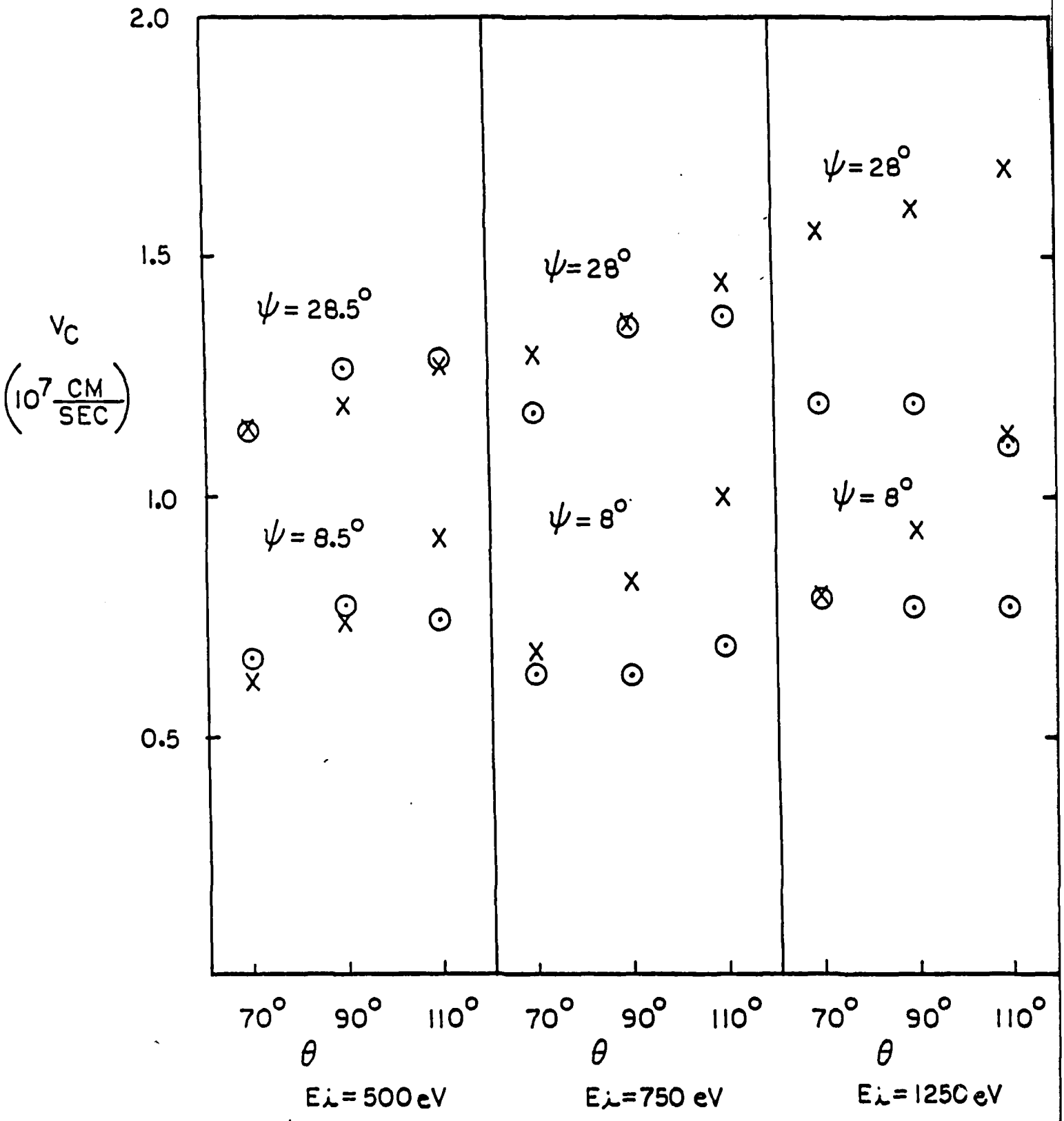
2.0
1.5
1.0
0.5
V_C
$\left(10^7 \frac{CM}{SEC}\right)$
$\psi = 28.5°$
$\psi = 8.5°$
$\psi = 28°$
$\psi = 8°$
$\psi = 28°$
$\psi = 8°$
70° 90° 110°
θ
70° 90° 110°
θ
70° 90° 110°
θ
$E_i = 500$ eV
$E_i = 750$ eV
$E_i = 1250$ eV

T. George ONR Technical Report Mailing List - 10/19/84

Office of Naval Research
Attn: Code 413
800 N. Quincy Street
Arlington, Virginia 22217

Dr. Bernard Douda
Naval Weapons Support Center
Code 5042
Crane, Indiana 47522

Defense Technical Information Center
Building 5, Cameron Station
Alexandria, Virginia 22314

Commander, Naval Air Systems
Command
Attn: Code 310C (H. Rosenwasser)
Washington, D.C. 20360

Dr. William Tolles
Superintendent
Chemistry Division, Code 6100
Naval Research Laboratory
Washington, D.C. 20375

Naval Civil Engineering Laboratory
Attn: Dr. R. W. Drisko
Port Hueneme, California 93401

Dr. David L. Nelson
Chemistry Division
Office of Naval Research
800 North Quincy Street
Arlington, Virginia 22217

DTNSRDC
Attn: Dr. G. Bosmajian
Applied Chemistry Division
Annapolis, Maryland 21401

Dr. J. Murday
Naval Research Laboratory
Surface Chemistry Division (6170)
455 Overlook Avenue, S.W.
Washington, D.C. 20375

Dr. David Young
Code 334
NORDA
NSTL, Mississippi 39529

T. George ONR Technical Report Mailing List - 10/19/84

Naval Weapons Center
Attn: Dr. Ron Atkins
Chemistry Division
China Lake, California 93555

Dr. G. A. Somorjai
Department of Chemistry
University of California
Berkeley, California 94720

Scientific Advisor
Commandant of the Marine Corps
Code RD-1
Washington, D.C. 20380

Dr. J. B. Hudson
Materials Division
Rensselaer Polytechnic Institute
Troy, New York 12181

U.S. Army Research Office
Attn: CRD-AA-IP
P.O. Box 12211
Research Triangle Park, NC 27709

Dr. Theodore E. Madey
Surface Chemistry Section
Department of Commerce
National Bureau of Standards
Washington, D.C. 20234

Mr. John Boyle
Maerials Branch
Naval Ship Engineering Center
Philadelphia, Pennsylvania 19112

Dr. J. E. Demuth
IBM Corporation
Thomas J. Watson Research Center
P.O. Box 218
Yorktown Heights, New York 10598

Naval Ocean Systems Center
Attn: Dr. S. Yamamoto
Marine Sciences Division
San Diego, California 91232

Dr. M. G. Lagally
Department of Metallurgical
and Mining Engineering
University of Wisconsin
Madison, Wisconsin 53706

T. George ONR Technical Report Mailing List - 10/19/84

Dr. R. P. Van Duyne
Department of Chemistry
Northwestern University
Evanston, Illinois 60201

Dr. W. T. Peria
Electrical Engineering Department
University of Minnesota
Minneapolis, Minnesota 55455

Dr. J. M. White
Department of Chemistry
University of Texas
Austin, Texas 78712

Dr. Keith H. Johnson
Department of Metallurgy
and Materials Science
Massachusetts Institute of Technology
Cambridge, Massachusetts 02139

Dr. D. E. Harrison
Department of Physics
Naval Postgraduate School
Monterey, California 93940

Dr. S. Sibener
Department of Chemistry
James Franck Institute
5640 Ellis Avenue
Chicago, Illinois 60637

Dr. W. Kohn
Department of Physics
University of California, San Diego
La Jolla, California 92037

Dr. Arnold Green
Quantum Surface Dynamics Branch
Code 3817
Naval Weapons Center
China Lake, California 93555

Dr. R. L. Park
Director
Center of Materials Research
University of Maryland
College Park, Maryland 20742

Dr. A. Wold
Department of Chemistry
Brown University
Providence, Rhode Island 02912

T. George ONR Technical Report Mailing List - 10/19/84

Dr. S. L. Bernasek
Department of Chemistry
Princeton University
Princeton, New Jersey 08544

Dr. R. Stanley Williams
Department of Chemistry
University of California
Los Angeles, California 90024

Dr. P. Lund
Department of Chemistry
Howard University
Washington, D.C. 20059

Dr. R. P. Messmer
Materials Characterization Lab
General Electric Company
Schenectady, New York 12301

Dr. F. Carter
Code 6132
Naval Research Laboratroy
Washington, D.C. 20375

Dr. Robert Gomer
Department of Chemistry
James Franck Institute
5640 Ellis Avenue
Chicago, Illinois 60637

Dr. Richard Colton
Code 6112
Naval Research Laboratory
Washington, D.C. 20375

Dr. Ronald Lee
R301
Naval Surface Weapons Center
White Oak
Silver Spring, Maryland 20910

Dr. Dan Pierce
Optical Physics Division
National Bureau of Standards
Washington, D.C. 20234

Dr. Paul Schoen
Code 5570
Naval Research Laboratory
Washington, D.C. 20375

T. George ONR Technical Report Mailing List - 10/19/84

Dr. John T. Yates
Department of Chemistry
University of Pittsburgh
Pittsburgh, Pennsylvnia 15260

Dr. Adam Heller
Bell Laboratories
Murray Hill, New Jersey 07974

Dr. Richard Greene
Code 5230
Naval Research Laboratory
Washington, D.C. 20375

Dr. Martin Fleischmann
Department of Chemistry
Southampton University
Southampton SO9 5NH
Hampshire, England

Dr. L. Kesmodel
Department of Physics
Indiana University
Bloomington, Indiana 47403

Dr. John W. Wilkins
Laboratory of Atomic and
Solid State Physics
Cornell University
Ithaca, New York 14853

Dr. K. C. Janda
California Institute of Technology
Division of Chemistry and
Chemical Engineering
Pasadena, California 91125

Dr. Richard Smardzewski
Code 6130
Naval Research Laboratory
Washington, D. C. 20375

Dr. E. A. Irene
Department of Chemistry
University of North Carolina
Chapel Hill, North Carolina 27514

Dr. H. Tachikawa
Department of Chemistry
Jackson State University
Jackson, Mississippi 39217

T. George ONR Technical Report Mailing List - 10/19/84

Dr. R. G. Wallis
Department of Physics
University of California
Irvine, California 92717

Dr. J. T. Keiser
Department of Chemistry
University of Richmond
Richmond, Virginia 23173

Dr. D. Ramaker
Department of Chemistry
George Washington University
Washington, D.C. 20052

Dr. Roald Hoffman
Department of Chemistry
Cornell University
Ithaca, New York 14853

Dr. J. C. Hemminger
Department of Chemistry
Universit of California
Irvine, California 92717

Dr. R. W. Plummer
Department of Physics
University of Pennsylvania
Philadelphia, Pennsylvania 19104

Dr. G. Rubloff
IBM
Thomas J. Watson Research Center
P.O. Box 218
Yorktown Heights, New York 10598

Dr. E. Yeager
Department of Chemistry
Case Western Reserve University
Cleveland, Ohio 41106

Dr. Horia Metiu
Department of Chemistry
University of California
Santa Barbara, California 93106

Dr. N. Winograd
Department of Chemistry
Pennsylvania State University
University Park, Pennsylvania 16802

T. George ONR Technical Report Mailing List - 10/19/84

Dr. M. Grunze
Laboratory for Surface Science
and Technology
University of Maine
Orono, Maine 04469

Dr. F. Kutzler
Department of Chemistry
Box 5055
Tennessee Technological University
Cookesville, Tennessee 38501

Dr. J. Butler
Naval Research Laboratory
Code 6115
Washington DC 20375

Dr. D. DiLella
Chemistry Department
George Washington University
Washington DC 20052

Dr. L. Interante
Chemistry Department
Renssealer Polytechnic Institute
Troy, New York 12181

Dr. R. Reeves
Chemistry Department
Renssaeler Polytechnic Institute
Troy NY 12181

Dr. Irvin Heard
Chemistry and Physics Department
Lincoln University
Lincoln University, Pennsylvania 19352

Dr. David young
Code 334
NORDA
NSTL, Mississippi 39529

Dr. K. J. Klaubunde
Department of Chemistry
Kansas State University
Manhattan, Kansas 66506

T. George ONR Technical Report Mailing List - 10/19/84

Dr. A. Steckl
Department of Electrical and
Systems Engineering
Rensselaer Polytechnic Institute
Troy, New York 12181

Dr. J. E. Jensen
Hughes Research Laboratory
3011 Malibu Canyon Road
Malibu, California 90265

Dr. G. H. Morrison
Department of Chemistry
Cornell University
Ithaca, New York 14853

Dr. J. H. Weaver
Department of Chemical Engineering
and Materials Science
University of Minnesota
Minneapolis, Minnesota 55455

Dr. P. Hansma
Department of Physics
University of California
Santa Barbara, California 93106

Dr. W. Knauer
Hughes Research Laboratory
3011 Malibu Canyon Road
Malilbu, California 90265

Dr. J. Baldeschwieler
Division of Chemistry
California Institute of Technology
Pasadena, California 91125

Dr. C. B. Harris
Department of Chemistry
University of California
Berkeley, California 94720

Dr. W. Goddard
Division of Chemistry
California Institute of Technology
Pasadena, Califlornia 91125

Dr. A. Reisman
Microelectronics Center
of North Carolina
Research Triangle Park
North Carolina 04469

END

FILMED

2-86

DTIC